GEOPHYSICS, VOL. 68, NO. 6 (NOVEMBER-DECEMBER 2003); P. 1857–1869, 12 FIGS.
10.1190/1.1635038

Simultaneous 1D inversion of loop–loop electromagnetic data for magnetic susceptibility and electrical conductivity

Colin G. Farquharson*, Douglas W. Oldenburg*, and Partha S. Routh‡

ABSTRACT

Magnetic susceptibility affects electromagnetic (EM) loop–loop observations in ways that cannot be replicated by conductive, nonsusceptible earth models. The most distinctive effects are negative in-phase values at low frequencies. Inverting data contaminated by susceptibility effects for conductivity alone can give misleading models: the observations strongly influenced by susceptibility will be underfit, and those less strongly influenced will be overfit to compensate, leading to artifacts in the model. Simultaneous inversion for both conductivity and susceptibility enables reliable conductivity models to be constructed and can give useful information about the distribution of susceptibility in the earth. Such information complements that obtained from the inversion of static magnetic data because EM measurements are insensitive to remanent magnetization.

We present an algorithm that simultaneously inverts susceptibility-affected data for 1D conductivity and susceptibility models. The solution is obtained by minimizing an objective function comprised of a sum-of-squares measure of data misfit and sum-of-squares measures of the amounts of structure in the conductivity and susceptibility models. Positivity of the susceptibilities is enforced by including a logarithmic barrier term in the objective function. The trade-off parameter is automatically estimated using the generalized cross validation (GCV) criterion. This enables an appropriate fit to the observations to be achieved even if good noise estimates are not available. As well as synthetic examples, we show the results of inverting airborne data sets from Australia and Heath Steele Stratmat, New Brunswick.

INTRODUCTION

Electromagnetic (EM) induction methods in geophysics are sensitive to the magnetic susceptibility of the earth as well as its electrical conductivity; the presence or absence of susceptible materials causes significant differences in the observed responses. For example, Figure 1a shows, as functions of frequency, the z-components of the secondary H-fields arising from a vertical magnetic dipole source above homogeneous half-spaces of differing susceptibilities. The survey geometry for this example mimics that of an airborne EM survey: the source and observation location are both 40 m above the surface of the half-space and 8.1 m apart. As seen in Figure 1a, both the in-phase and quadrature responses go to zero as the frequency decreases when the half-space is not susceptible. If the half-space is susceptible, the low-frequency asymptote of the in-phase component is negative, and its value becomes more negative as the susceptibility increases. Figure 1b shows the frequency dependence of the x-component of the secondary H-field for an x-directed magnetic dipole source (for the same airborne configuration as for Figure 1a; the transmitter–receiver separation is in the x-direction). The differences caused in this response by different susceptibilities of the half-space are similar to those for the vertical dipole arrangement: the low-frequency asymptote of the in-phase component is zero for zero susceptibility and becomes more significant, in a sense opposite to that of its high-frequency asymptote, as the susceptibility of the half-space increases. In contrast, the quadrature components shown in both Figures 1a and 1b are much less strongly influenced by the susceptibility of the half-space.

The influence of susceptible materials on the responses of EM induction systems also depends on the geometry of the transmitter–receiver pair. Figure 2 shows how the z-component of the secondary H-field for a z-directed magnetic dipole source varies, at low frequency (110 Hz), as a function of both

Manuscript received by the Editor July 26, 2001; revised manuscript received March 18, 2003.
*University of British Columbia, Geophysical Inversion Facility, Department of Earth and Ocean Sciences, 6339 Stores Rd., Vancouver, British Columbia V6T 1Z4, Canada. E-mail: farq@eos.ubc.ca; doug@eos.ubc.ca.
‡Boise State University, Department of Geosciences, Boise, Idaho 89725. E-mail: prouth@boisestate.edu.

the separation between the source and observation location and the height of the source–receiver pair above a homogeneous half-space. Figures 2a and 2b show the in-phase and quadrature components of the response over a susceptible (0.1 SI units) and conductive (0.001 S/m) half-space; Figures 2c and 2d show the in-phase and quadrature components of the response over a half-space that is just conductive (0.001 S/m). The in-phase response over the susceptible half-space varies from large and positive for large source–receiver separations close to the half-space surface, to large and negative when the height of the source–receiver pair is similar to its separation, to small and negative for large heights but small separations. The in-phase response over the nonsusceptible half-space (Figure 2c) is considerably smaller than that over the susceptible half-space. It is also clear from Figure 2 that the quadrature component at this low frequency is hardly affected by the susceptibility of the earth model.

The nonzero values of the in-phase component of the secondary H-field at low frequencies as a result of the presence of susceptible materials cannot be reproduced by a conductive, nonmagnetic earth model. This is because the values of the in-phase component at low frequencies for such a model, no matter what the conductivity, are orders of magnitude smaller than those when susceptible materials are present. Not even with a 3D conductivity structure can significant values of the low-frequency response be modelled; the secondary fields go to zero as the frequency goes to zero, just as for a 1D model (see, e.g., Wait, 1953).

Any attempt to invert data contaminated with susceptibility effects for conductivity will be unsuccessful: it is impossible to reproduce the observations, and one will not know whether features in the constructed conductivity model are real or artifacts introduced to fit the susceptibility effects. Figure 3 shows a line of airborne EM data with negative values of the normalized

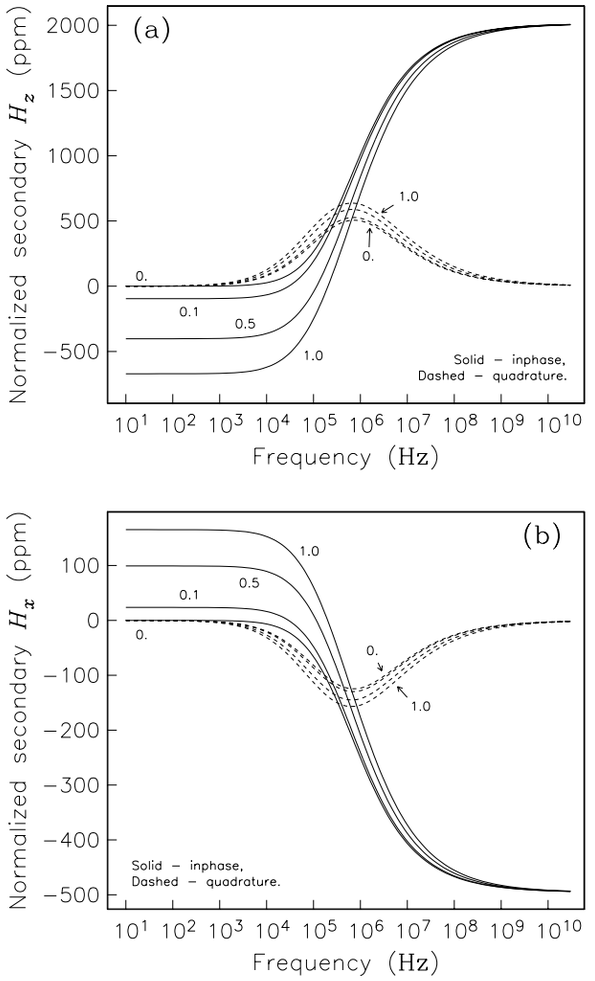

FIG. 1. (a) The z-component of the secondary H-field for a vertical magnetic dipole source over a homogeneous half-space of conductivity 0.001 S/m and variable susceptibility: 0, 0.1, 0.5, and 1.0 SI units. The source and observation location are 40 m above the half-space and are separated by 8.1 m. The field values have been normalized by the z-component of the free-space H-field. (b) The x-component of the secondary H-field for an x-directed magnetic dipole source above a half-space of the same conductivity and susceptibilities as for (a). The source and observation locations are also 40 m above the half-space and are separated by 8.1 m in the x-direction. The field values have been normalized by the x-component of the free-space H-field for this transmitter-receiver orientation.

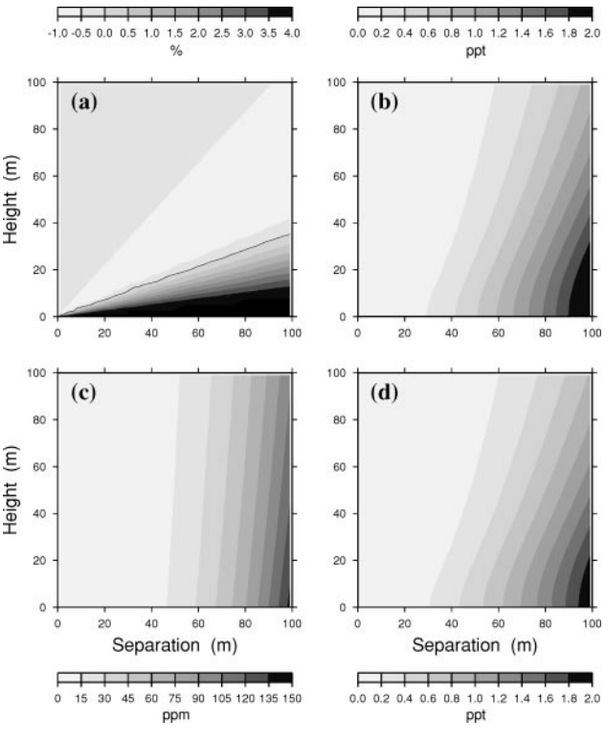

FIG. 2. The z-component of the secondary H-field for a z-directed magnetic dipole source above a homogeneous half-space as a function of the separation between the source and observation location and the height of both source and observation location above the half-space's surface. (a) In-phase and (b) quadrature components for a half-space that is both conductive (0.001 S/m) and susceptible (0.1 SI units). (c) In-phase and (d) quadrature components for a half-space that is conductive only (0.001 S/m). The frequency was 110 Hz. The secondary field values have been normalized by the free-space H-field for the relevant separations. Note the different scales (ppm = parts per million; ppt = parts per thousand). The single contour line in (a) indicates zero secondary field. Above this line the normalized secondary H_z is negative; below it, positive.

in-phase component at low frequencies. These data are values of the vertical component of the H-field generated by a vertical magnetic dipole source at 1325, 4925, and 11 025 Hz. The separation between the source and receiver was 5.1 m along the flight line, and their height was approximately 33 m above the earth's surface. The values of the secondary field have been normalized by the free-space field. The model constructed by inverting the six data points (in-phase and quadrature components at the three frequencies) at each location along the line for a 1D conductive, but nonsusceptible, model is shown in Figure 3c. The forward-modelled data for this model are shown in Figure 3a, from which we see they fail considerably to match the observations.

From Figures 1 and 2, we deduce there are not such fundamental differences in the quadrature responses for susceptible and nonsusceptible models as there are in the in-phase responses. Figure 4 shows the results of inverting only the quadrature components of the airborne data shown in Figure 3 for a conductive, nonsusceptible model. As Figure 4a indicates, the observed quadrature responses are successfully reproduced by those computed for the model generated by the inversion (Figure 4c).

If the goal is to determine only the electrical conductivity structure of the earth, Figure 4 shows that a first approximation can be obtained from a set of susceptibility-contaminated observations by ignoring their in-phase components. However, this involves throwing away half a data set, and uncertainty remains over the reliability of features in the constructed conductivity model since the effect of susceptibility on the quadrature components is not completely negligible (see Figure 1). Hence, even if the susceptibility distribution within the earth is not of interest, an inversion algorithm that properly takes into account the effects of susceptibility will produce a more reliable conductivity model and will enable all the acquired data to be used in the inversion. Such an algorithm is required, of course, if knowledge of the variation of susceptibility within the earth is desired as well as that of conductivity. Information about the susceptibility structure of the earth determined from EM induction data is not influenced by any remanent magnetization, and so provides complementary information to that obtained from inverting observations of the static magnetic field. It is an inversion algorithm that can simultaneously construct models of the vertical variation of susceptibility and conductivity within the earth from EM induction data that we present in this paper.

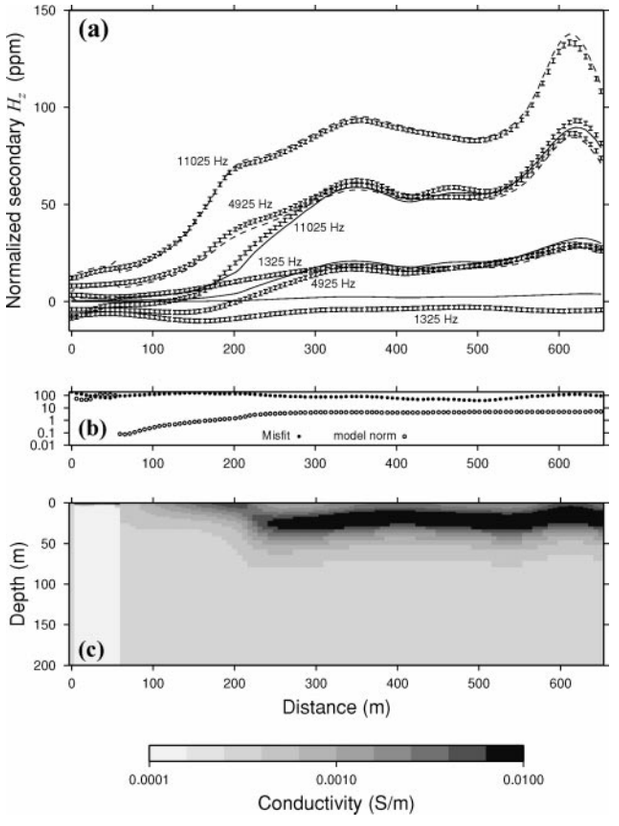

FIG. 3. The result of inverting a line of airborne EM data with obvious susceptibility effects for an earth model that is conductive but not susceptible. (a) Dots and error bars represent the observations. The lines are the data forward-modelled from the model produced by the inversion. The solid and dashed lines indicate the in-phase and quadrature parts, respectively, of the responses. The observations were for the horizontal coplanar coil configuration. Data were collected at three frequencies: 1325, 4925 and 11 025 Hz. (b) Data misfit (filled circles) and model structure term (open circles). (c) Final conductivity model (comprised of all 1D models below each measurement location).

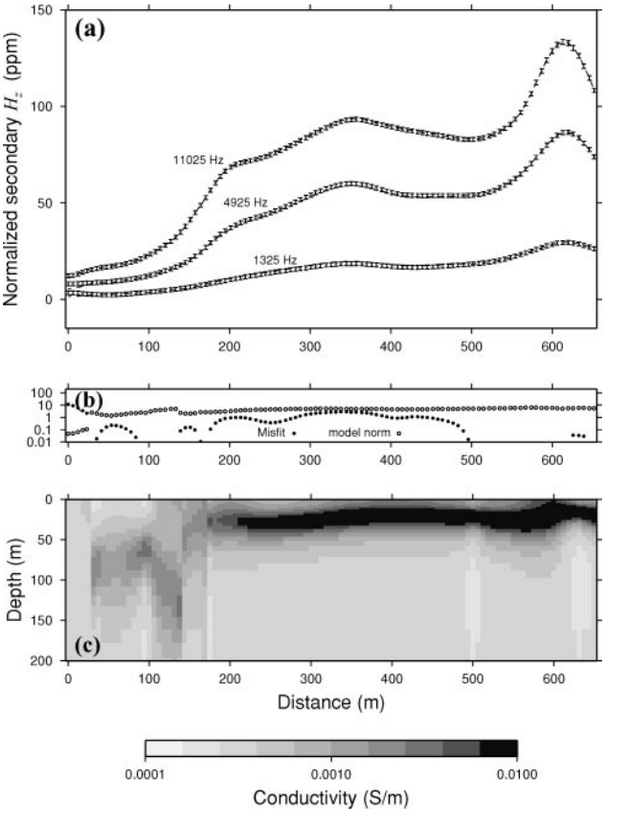

FIG. 4. The result of inverting only the quadrature components of the airborne data shown in Figure 3 for a conductive but nonsusceptible earth model. (a) Observations (dots and error bars) and forward-modelled data (dashed lines) for the final model. (b) Misfit (filled circles) and model norm (open circles). (c) Final conductivity model.

The inversion program we put forth has the same ultimate goal and shares the same basic philosophy as the procedure presented by Zhang and Oldenburg (1999): both pose the inverse problem as an optimization problem in which an objective function comprising a measure of data misfit and measures of the structure in the conductivity and susceptibility models is minimized. However, the components of our method are done differently and in ways that we consider improvements upon those of Zhang and Oldenburg. We consider any possible orientation of the magnetic dipole source and any or all components of the resulting H-field at one or more locations relative to each source. Also, the observations can be any combination of the in-phase and/or quadrature measurements. Our forward-modeling algorithm uses a matrix propagation technique, and we compute the elements of the Jacobian matrix of sensitivities using a sensitivity-equation approach based on the direct differentiation of the equations of the forward-modeling algorithm. This is an inherently stable process, unlike a method that requires propagation of fields or potentials back down through a layered model, and our implementation is just as efficient as the adjoint-equation approach. We also implement two recent advances in geophysical inverse theory: generalized cross validation (GCV) and L-curve criteria for automatically determining the trade-off between the misfit and model structure terms in the objective function. These are particularly useful when, as is often the case, the amount of noise in a set of observations is unknown. Finally, to ensure positivity (if desired) of the constructed susceptibility model, our method incorporates a logarithmic barrier term in the objective function (which we prefer to the nonlinear transformation used by Zhang and Oldenburg).

We, along with Zhang and Oldenburg (1999), are not the first to propose a way of obtaining both conductivity and susceptibility information from EM data. Beard and Nyquist (1998) compute the best-fitting conductivity and susceptibility of a homogeneous half-space from frequency-domain data; Huang and Fraser (1998, 2000) calculate apparent resistivities and susceptibilities, also from frequency-domain data; and Zhdanov and Pavlov (2001) generate 1D pseudosections of conductivity and susceptibility from time-domain data.

We first describe the various components of our inversion program, illustrating the important aspects by its application to a set of synthetic data. Then, we illustrate its performance by discussing the results obtained from inverting two field data sets: the one shown in Figures 3 and 4 and one acquired over the massive sulfide deposit at Heath Steele Stratmat, New Brunswick.

FORWARD MODELING AND SENSITIVITY CALCULATIONS

Our models of the vertical variation of conductivity and susceptibility within the earth are composed of horizontal, uniform layers. During an inversion, the depths of the layer interfaces remain fixed; the susceptibility and the logarithm of the conductivity within each layer are sought. To compare with observations, we need to be able to calculate any or all of the components of the H-field anywhere above the surface of the model generated by horizontal and/or vertical magnetic dipole sources, also anywhere above the surface of the model. Our procedure is based on the matrix propagation method of Farquharson and Oldenburg (1996). All of the matrices for the individual layers and the matrix products computed in the course of the forward modeling are saved for reuse in the sensitivity computations.

The relationship between the conductivities and susceptibilities in the model and the observations is nonlinear. To solve the subsequent nonlinear inverse problem, we use an iterative procedure, at each iteration of which we solve a linearized approximation of the full problem. This requires the ability to calculate the Jacobian matrix of sensitivities. Our procedure for doing this is derived from the direct differentiation, with respect to the model parameters, of the equations of the forward-modeling algorithm (see the Appendix). This is an efficient technique because most of the quantities required by the sensitivity-computing algorithm have been previously calculated and saved during a call to the forward-modeling routine and are reused in computing the sensitivities. This is significant because generating the Jacobian matrix is the single most time-consuming part of the inversion algorithm.

Examples of sensitivities for airborne-type data over a homogeneous half-space of conductivity 0.001 S/m and zero susceptibility are shown in Figure 5. Data at five frequencies were considered: 880, 7213, 55 840, 1082, and 5848 Hz. For the first three frequencies, the transmitter was a vertical magnetic dipole and the data were the vertical component of the H-field (the so-called horizontal coplanar configuration). For the final two frequencies, the transmitter was an x-directed dipole and the data were the x-component of the H-field (coaxial configuration). The transmitter and observation location were both at a height of 40 m for all five frequencies and were separated by 8.1 m (6.3 m for the 56-kHz coils) in the x-direction. (These configurations and the half-space conductivity are the same as for Figure 1.) The sensitivities were computed for 32 layers whose thicknesses increased with depth by a factor of 1.1 from an initial thickness of 1 m. The sensitivities are plotted at the centers of their respective layers.

From Figure 5 we can see that the sensitivities of the in-phase components with respect to the layer susceptibilities are considerably larger than the other three types of sensitivities, which all have similar ranges. Figure 5b (in particular, the three frequencies for the horizontal coplanar configuration) also shows that the sensitivities of the in-phase components with respect to the susceptibilities are larger at the lower frequencies. This is in contrast to all the other sensitivities. The sensitivities of the in-phase components with respect to the susceptibilities, for both transmitter–receiver configurations, are of the opposite sign to the corresponding components of the secondary H-field (see Figure 1), again in contrast to the other sensitivities, which are predominantly of the same sign as the corresponding field values. Increasing the susceptibilities in a model, especially in the layers near the surface for which the sensitivities are larger, therefore decreases the in-phase components of the data—considerably so because of the large relative size of these sensitivities. Also, because the sensitivities of the in-phase component with respect to the logarithms of the layer conductivities are mostly positive, a decrease in conductivity (and a large decrease because of the logarithm) is required to decrease the in-phase component if, for example, one is attempting to fit susceptibility-affected data by inverting for conductivity alone. This can result in excessively resistive features within the constructed conductivity model. Finally, the sensitivities for a half-space of the same conductivity but of 0.1 SI units

susceptibility were not noticeably different from those shown in Figure 5, except for the sensitivities of the in-phase components with respect to the layer susceptibilities, which had the same depth dependence but were about 10% smaller.

THE INVERSION PROCEDURE

The algorithm

The goal of the inversion is to construct the simplest model that adequately fits the observations. This is accomplished by posing the inverse problem as an optimization problem in which the earth model that minimizes the objective function

$$\Phi = \phi_d + \beta\phi_m - \gamma\phi_{LB} \tag{1}$$

is sought. Here, ϕ_d is the typical sum-of-squares measure of data misfit:

$$\phi_d = \left\| \mathbf{W}_d(\mathbf{d} - \mathbf{d}^{\text{obs}}) \right\|^2, \tag{2}$$

where $\|\cdot\|$ indicates the l_2-norm, $\mathbf{d}^{\text{obs}}$ is the vector containing N observations, and $\mathbf{d}$ is the vector of forward-modelled data for the earth model. The in-phase and quadrature components for any particular frequency and source–receiver geometry are considered as two separate, independent data values. We assume that the noise in the observations is Gaussian and uncorrelated. Therefore, $\mathbf{W}_d$ is a diagonal matrix whose elements are the reciprocals of the (estimated) standard deviations of the noise in the observations. The single model-structure component in the objective function Φ is actually made up of four terms:

$$\begin{aligned}\phi_m = {} & \alpha_s^\sigma \left\| \mathbf{W}_s^\sigma \left(\mathbf{m}^\sigma - \mathbf{m}_s^{\sigma,\text{ref}}\right) \right\|^2 + \alpha_z^\sigma \left\| \mathbf{W}_z^\sigma \left(\mathbf{m}^\sigma - \mathbf{m}_z^{\sigma,\text{ref}}\right) \right\|^2 \\ & + \alpha_s^\kappa \left\| \mathbf{W}_s^\kappa \left(\mathbf{m}^\kappa - \mathbf{m}_s^{\kappa,\text{ref}}\right) \right\|^2 + \alpha_z^\kappa \left\| \mathbf{W}_z^\kappa \left(\mathbf{m}^\kappa - \mathbf{m}_z^{\kappa,\text{ref}}\right) \right\|^2,\end{aligned} \tag{3}$$

where $\mathbf{m}^\sigma$ is the vector containing the logarithms of the conductivities of the M layers (including the basement half-space) and $\mathbf{m}^\kappa$ is the vector containing the susceptibilities of the M layers. The matrices $\mathbf{W}_s^\sigma$ and $\mathbf{W}_s^\kappa$ are diagonal matrices whose elements are equal to the square roots of the layer thicknesses, unless weighting certain parts of the model relative to others is preferred for a particular inversion. The matrices $\mathbf{W}_z^\sigma$ and $\mathbf{W}_z^\kappa$ are the first-order, finite-difference operators whose rows are scaled by the reciprocals of the square roots of half the distance between the centers of the two respective layers—again, unless a specific relative weighting between parts of the model is required. [See, for example, Farquharson and Oldenburg (1993) for explicit descriptions of these four weighting matrices.] The vectors $\mathbf{m}_s^{\sigma,\text{ref}}$, $\mathbf{m}_z^{\sigma,\text{ref}}$, $\mathbf{m}_s^{\kappa,\text{ref}}$, and $\mathbf{m}_z^{\kappa,\text{ref}}$, contain the parameters of the four possible reference models. The four terms in equation (3) therefore correspond to smallest and flattest terms for both the conductivity and susceptibility parts of the model. The choice of the relative weighting of these four terms, which is determined by the values of the coeffcients α_s^σ, α_z^σ, α_s^κ, and α_z^κ, is discussed later. The parameter β determines the balance

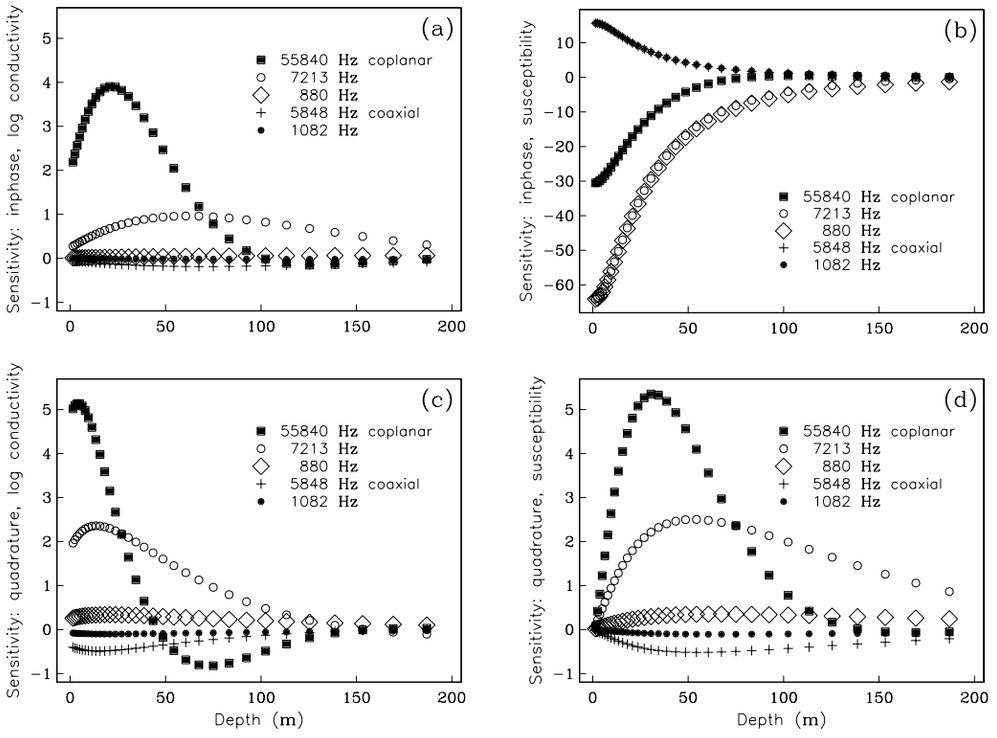

FIG. 5. Example sensitivities for airborne data with respect to both the (logarithms of the) conductivities and the susceptibilities of the layers within a homogeneous model. Sensitivities of the in-phase components with respect to the logarithms of (a) the layer conductivities and (b) the layer susceptibilities. (c), (d) Sensitivities of the quadrature components. Five frequencies are considered: 880 (◊), 7213 (○), 55 840 (■), 1082 (●), and 5848 Hz (+). The first three frequencies are for the horizontal coplanar coil configuration; the others are for the coaxial configuration. The sensitivities have been normalized by the free-space H-fields. The sensitivities of the in-phase component with respect to the susceptibilities are plotted on a different scale from the other three panels.

between the data misfit and model-structure component of the objective function, hence the trade-off between fitting the observations more closely and keeping the constructed model as simple as possible. How we choose this trade-off parameter is described in the following section. Finally, the third component of the objective function is a logarithmic barrier term:

$$\phi_{LB} = \sum_{j=1}^{M} \log \kappa_j, \tag{4}$$

where κ_j is the susceptibility of the jth layer. We expect the susceptibilities in all situations we consider to be less than one, meaning the terms in the above summation are always negative. Hence, the minus sign preceding this term in the objective function [equation (1)]. The size of ϕ_{LB} increases dramatically if the susceptibility of any layer approaches zero, so an algorithm searching for the minimum of an objective function containing a term like ϕ_{LB} avoids models with such layers. This component of the objective function, including its coeffcient γ, is discussed later.

As mentioned, the inverse problem is nonlinear. We therefore construct an iterative procedure, at each iteration of which we solve a linearized approximation of the true inverse problem. At the nth iteration, we search for a perturbation $\delta\mathbf{m}$ to the current model $\mathbf{m}^{n-1}$ so that the linearized objective function

$$\Phi^n = \phi_d^n + \beta^n \phi_m^n - \gamma^n \phi_{LB}^n \tag{5}$$

is minimized. In this linearized objective function, the forward-modelled data in the misfit term ϕ_d^n are approximated by the first two terms in the Taylor series expansion:

$$\mathbf{d}^n = \mathbf{d}^{n-1} + \mathbf{J}^{\sigma,n-1}\delta\mathbf{m}^{\sigma} + \mathbf{J}^{\kappa,n-1}\delta\mathbf{m}^{\kappa}, \tag{6}$$

where $\delta\mathbf{m}^{\sigma} = \mathbf{m}^{\sigma,n} - \mathbf{m}^{\sigma,n-1}$, $\delta\mathbf{m}^{\kappa} = \mathbf{m}^{\kappa,n} - \mathbf{m}^{\kappa,n-1}$, and $\mathbf{J}^{\kappa,n-1}$ and $\mathbf{J}^{\sigma,n-1}$ are the Jacobian matrices of sensitivities with respect to the logarithms of the layer conductivities and the layer susceptibilities, respectively:

$$J_{ij}^{\sigma,n-1} = \left.\frac{\partial d_i}{\partial \log \sigma_j}\right|_{\mathbf{m}^{n-1}} \tag{7}$$

and

$$J_{ij}^{\kappa,n-1} = \left.\frac{\partial d_i}{\partial \kappa_j}\right|_{\mathbf{m}^{n-1}}. \tag{8}$$

The problem becomes that of finding the change, $(\delta\mathbf{m}^{\sigma T}\delta\mathbf{m}^{\kappa T})^T$, to the model that minimizes the (linearized) objective function, Φ^n. Differentiating Φ^n with respect to $\delta\mathbf{m}^{\sigma}$ and $\delta\mathbf{m}^{\kappa}$ and equating the resulting expressions to zero gives the system of equations to be solved. We differentiate the misfit and model-structure terms in Φ^n in the usual manner. However, an approximation must be introduced after differentiation of the logarithmic barrier term to give an expression that is linear in $\delta\mathbf{m}^{\kappa}$:

$$\frac{\partial \phi_{LB}^n}{\partial \delta m_k^{\kappa}} = \frac{\partial}{\partial \delta\kappa_k} \sum_{j=1}^{M} \log\left(\kappa_j^{n-1} + \delta\kappa_j\right) \tag{9}$$

$$= \frac{1}{\kappa_k^{n-1} + \delta\kappa_k} \tag{10}$$

$$\approx \frac{1}{\kappa_k^{n-1}}\left(1 - \frac{\delta\kappa_k}{\kappa_k^{n-1}}\right). \tag{11}$$

This approximation (obtained by keeping only the first two terms in the binomial expansion of $(1+\delta\kappa_k/\kappa_k^{n-1})^{-1}$) is valid for small $|\delta\kappa_k/\kappa_k^{n-1}|$. The linear system of equations to be solved for $(\delta\mathbf{m}^{\sigma T}\delta\mathbf{m}^{\kappa T})^T$ is therefore

$$\left[\mathbf{J}^{n-1T}\mathbf{W}_d^T\mathbf{W}_d\mathbf{J}^{n-1} + \beta^n \sum_{i=1}^{2}\mathbf{W}_i^T\mathbf{W}_i + \frac{\gamma^n}{2}\hat{\mathbf{X}}^{n-1T}\hat{\mathbf{X}}^{n-1}\right]\delta\mathbf{m}$$
$$= \mathbf{J}^{n-1T}\mathbf{W}_d^T\mathbf{W}_d(\mathbf{d}^{\text{obs}} - \mathbf{d}^{n-1}) + \beta^n \sum_{i=1}^{2}\mathbf{W}_i^T\mathbf{W}_i$$
$$\times\left(\mathbf{m}_i^{\text{ref}} - \mathbf{m}^{n-1}\right) + \frac{\gamma^n}{2}\hat{\mathbf{X}}^{n-1T}\hat{\mathbf{X}}^{n-1}\mathbf{m}^{n-1}, \tag{12}$$

where

$$\mathbf{J}^{n-1} = (\mathbf{J}^{\sigma,n-1}\mathbf{J}^{\kappa,n-1}), \tag{13}$$

$$\mathbf{W}_1 = \begin{pmatrix} \sqrt{\alpha_s^{\sigma}}\,\mathbf{W}_s^{\sigma} & 0 \\ 0 & \sqrt{\alpha_s^{\kappa}}\,\mathbf{W}_s^{\kappa} \end{pmatrix}, \tag{14}$$

$$\mathbf{W}_2 = \begin{pmatrix} \sqrt{\alpha_z^{\sigma}}\,\mathbf{W}_z^{\sigma} & 0 \\ 0 & \sqrt{\alpha_z^{\kappa}}\,\mathbf{W}_z^{\kappa} \end{pmatrix}, \tag{15}$$

$$\mathbf{m}_1^{\text{ref}} = \left(\mathbf{m}_s^{\sigma,\text{ref}\,T}\mathbf{m}_s^{\kappa,\text{ref}\,T}\right)^T,$$
$$\mathbf{m}_2^{\text{ref}} = \left(\mathbf{m}_z^{\sigma,\text{ref}\,T}\mathbf{m}_z^{\kappa,\text{ref}\,T}\right)^T,$$

and

$$\hat{\mathbf{X}}^{n-1} = (0 \quad (\mathbf{X}^{n-1})^{-1}), \tag{16}$$

where $\mathbf{X}^{n-1} = \text{diag}\{m_1^{\kappa,n-1}, \ldots, m_M^{\kappa,n-1}\}$.

The solution to equation (12) is equivalent to the least-squares solution of

$$\begin{pmatrix} \mathbf{W}_d\mathbf{J}^{n-1} \\ \sqrt{\beta^n}\,\mathbf{W}_1 \\ \sqrt{\beta^n}\,\mathbf{W}_2 \\ \sqrt{\frac{\gamma^n}{2}}\hat{\mathbf{X}}^{n-1} \end{pmatrix}\delta\mathbf{m} = \begin{pmatrix} \mathbf{W}_d(\mathbf{d}^{\text{obs}} - \mathbf{d}^{n-1}) \\ \sqrt{\beta^n}\,\mathbf{W}_1\left(\mathbf{m}_1^{\text{ref}} - \mathbf{m}^{n-1}\right) \\ \sqrt{\beta^n}\,\mathbf{W}_2\left(\mathbf{m}_2^{\text{ref}} - \mathbf{m}^{n-1}\right) \\ \sqrt{\frac{\gamma^n}{2}}\hat{\mathbf{X}}^{n-1}\mathbf{m}^{n-1} \end{pmatrix}, \tag{17}$$

which we solve using the LSQR routine of Paige and Saunders (1982). This is slightly more efficient than solving equation (12) directly.

Once $\delta\mathbf{m}$ has been determined, the new model is given by

$$\mathbf{m}^n = \mathbf{m}^{n-1} + \lambda\delta\mathbf{m}, \tag{18}$$

where $\lambda \in (0, 1]$. The restriction that the susceptibilities must be nonnegative means that the condition

$$\lambda\delta\kappa_j > -\kappa_j^{n-1} \tag{19}$$

must hold for all $j = 1, \ldots, M$. In addition, consistency with the linear approximation in equation (11) requires that $\delta\kappa_j > -\kappa_j^{n-1}$. We therefore choose the initial value of the step length λ for the nth iteration to be the largest value allowed by equation (19), or 1, whichever is smaller. Also, the objective function must be decreased by the chosen value of λ. For the resulting model $\mathbf{m}^n(\lambda)$, we compute the data $\mathbf{d}^n(\lambda)$ [using the full forward modeling, not the linearized approximation given by equation (6)] and hence the misfit $\phi_d^n(\lambda)$ for this value of the

step length. For this model, we also compute the model structure and logarithmic barrier terms: $\phi_m^n(\lambda)$ and $\phi_{LB}^n(\lambda)$. We then compare the value of the objective function with the value of the equivalent objective function for the previous iteration to ensure the condition

$$\phi_d^n(\lambda) + \beta^n \phi_m^n(\lambda) - \gamma^n \phi_{LB}^n(\lambda) < \phi_d^{n-1} + \beta^n \phi_m^{n-1} - \gamma^n \phi_{LB}^{n-1} \tag{20}$$

is true. If equation (20) does not hold, λ is decreased by factors of two until equation (20) is satisfied.

Finally, to determine when the algorithm has converged, we use the criteria (Gill et al., 1981)

$$\Phi^{n-1} - \Phi^n < \tau(1 + \Phi^n), \tag{21}$$

$$\|\mathbf{m}^{n-1} - \mathbf{m}^n\| < \sqrt{\tau}(1 + \|\mathbf{m}^n\|), \tag{22}$$

where τ is specified by the user but is usually $\sim$0.01.

Choosing the trade-off parameter

The ultimate value of the trade-off parameter β should be such that the observations are reproduced as closely as possible without fitting the noise. If the noise in a set of observations is known, the trade-off parameter can be chosen using a univariate search so that the value of the misfit ϕ_d for the model constructed by the inversion is equal to its expectation, $E(\phi_d)$. In practice, however, estimates of the noise are not usually made, meaning that $E(\phi_d)$ is unknown.

A number of automatic methods exist for estimating, during the course of an inversion, a value of the trade-off parameter that will give a suitable fit to the observations, for example, the generalized cross-validation criterion (GCV) (e.g., Wahba, 1990; Haber and Oldenburg, 2000), the L-curve criterion (e.g., Hansen, 1998; Li and Oldenburg, 1999), and Akaike's Bayesian information criterion (e.g., Uchida, 1993; Mitsuhata and Uchida, 2000). The examples we present use the GCV criterion. (For more information, see Farquharson and Oldenburg, 2003).

Irrespective of the approach used to determine the trade-off parameter, experience shows that a conservative implementation is the most reliable. Our initial model is usually a homogeneous half-space, and we limit the change in the model at each iteration so structure is introduced gradually. This is consistent with the linearized approximation of the true inverse problem being solved at each iteration. We choose the initial value of the trade-off parameter such that $\beta^1 \phi_m^* = \phi_d^0$, where ϕ_d^0 is the misfit for the starting model and ϕ_m^* is the value of the model structure term calculated for a model thought to represent the expected geological structure, not the starting model. At each iteration, we restrict the decrease in the trade-off parameter to be, at most, a factor of 10. The resulting behavior of the trade-off parameter is therefore essentially that for a cooling schedule whose asymptote is determined during the course of the inversion.

Figure 6 shows the results of the inversion of a synthetic data set. The data were again for an airborne configuration: five frequencies, three of which (880, 7213, and 55 840 Hz) were for a vertical magnetic dipole source and measurements of the z-component of the secondary H-field and two of which (1082 and 5848 Hz) were for an x-directed dipole source and measurements of the x-component of the secondary H-field. Both the transmitter and receiver were at a height of 40 m and were separated by 8.1 m in the x-direction for both configurations (except for the highest frequency for which the separation was 6.3 m). Forward-modelled data were computed for the model shown by the dashed lines in Figures 6b and 6c, to which Gaussian noise with zero mean was added. The values of the secondary fields were normalized by the free-space fields for the respective transmitter–receiver configurations. The standard deviation of the noise added to each datum was equal to 5% of the magnitude of the datum, unless this was less than 1 ppm, in which case 1 ppm was used. This was considered to be a reasonable representation of the noise in an actual airborne survey. The synthetic data are indicated by the error bars in Figure 6a. The solid and dashed lines in Figure 6a show the in-phase and quadrature components of the forward-modelled data for the model constructed by the inversion. The conductivity and susceptibility parts of this model are shown by the solid lines in Figures 6b and 6c.

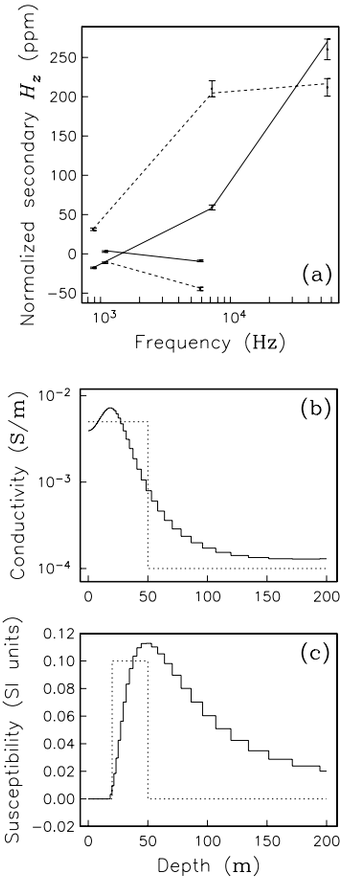

FIG. 6. The results of inverting the synthetic data set described in the text. These data are indicated by the error bars in (a). The models from which the data were generated are indicated by the dashed lines in (b) and (c). The first, fourth and fifth frequencies are for the horizontal coplanar coil configuration, and the second and third are for the coaxial configuration. The solid and dashed lines in (a) indicate the forward-modelled in-phase and quadrature data, respectively, for the model constructed by the inversion. The conductivity and susceptibility components of the model are shown by the solid lines in (b) and (c).

Figure 7 shows the changes in the components of the objective function Φ during the inversion of the synthetic data set shown in Figure 6. Fifty layers were in the model (including the basement half-space), with the depth to the top of the basement half-space equal to 400 m. The starting model was a homogeneous half-space of conductivity 0.007 S/m and susceptibility 0.02 SI units. The reference model for the smallest components of the model structure term was a homogeneous half-space of conductivity 0.001 S/m (equal to the conductivity of the basement half-space in the model for which the data were generated) and zero susceptibility. The reference models for the flattest components were equal to zero. The trade-off parameter β was chosen at each iteration by the GCV-based approach. It was not allowed to decrease by more than a factor of two at any one iteration. This restriction determined the variation of β for the first five iterations, as can be seen from Figure 7. We can also see that the misfit steadily decreased before leveling out at the value resulting from the GCV-based choice of β. The final value of misfit is equal to 5.4. The χ^2 measure of the amount of noise that was actually introduced into the synthetic data was equal to 7.5. The value of the trade-off parameter chosen by the inversion algorithm has therefore resulted in the observations being somewhat overfit, but certainly not to such an extent that the fit is not acceptable.

The relative weighting of conductivity and susceptibility

The values of the four coefficients α_s^σ, α_z^σ, α_s^κ, and α_z^κ in the model structure component of the objective function are ultimately the responsibility of the user, especially the ratios $R^\sigma = \alpha_z^\sigma / \alpha_s^\sigma$ and $R^\kappa = \alpha_z^\kappa / \alpha_s^\kappa$, which determine the relative emphasis on the smallness and flatness of the conductivity and susceptibility models, respectively. At present, we have nothing better than an ad hoc method for choosing the balance between R^σ and R^κ that is similar to the argument in the previous section for determining the starting value of the trade-off parameter. We compute the four components of ϕ_m in equation (3) for simple conductivity and susceptibility models that are reasonably representative of the area of interest, for example, a two-layer model with conductivities of 10^{-1} S/m over 10^{-2} S/m and susceptibilities of 0.02 SI units over zero. After having chosen the ratios R^σ and R^κ, we choose the balance R^σ / R^κ so the conductivity and susceptibility halves of ϕ_m are equal for the representative models. The ratios of the coefficients given by this argument are usually acceptable as initial estimates but should be further refined by the user so the final model is appropriate, given what is known about the geology of the region under investigation.

The values of the various coefficients in ϕ_m for the inversion whose results are shown in Figure 6 are $\alpha_z^\sigma = 1$, $\alpha_s^\sigma = 0.003$, $\alpha_z^\kappa = 0.9$, and $\alpha_s^\kappa = 0.063$, corresponding to a balance between the coefficients of the conductivity and susceptibility parts of ϕ_m of $R^\sigma / R^\kappa = 1.11$. Figure 8 shows the models constructed by the inversion of the same synthetic data using a value of $R^\sigma / R^\kappa = 0.02$. All other parameters in the inversion are the same, and the final misfit is the same to two significant figures (5.4). It is clear from Figure 8 that the conductivity model is almost identical to that in Figure 6b, but the susceptibility model is considerably different: all of the susceptible material is concentrated up near the surface and is of a much smaller value. This is typical if the susceptibility part of the model structure term is too large. The relative insensitivity of the conductivity model to the ratio R^σ / R^κ is also typical of the simultaneous inversion for both conductivity and susceptibility.

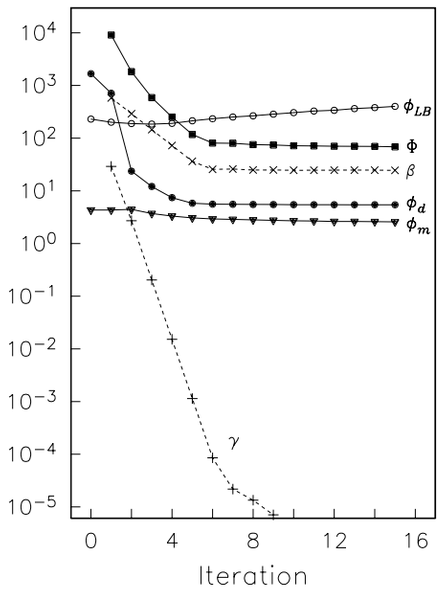

FIG. 7. The variation of the components of the objective function during the course of the inverse whose results are shown in Figure 6.

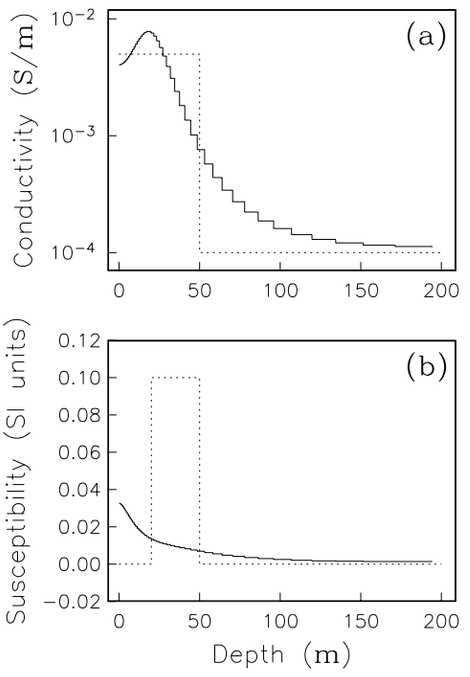

FIG. 8. The constructed models [solid lines; (a) conductivity, (b) susceptibility] for the inversion of the synthetic data set shown in Figure 6a using a value of 0.02 for the ratio R^σ / R^κ (instead of 1.11 for the results shown in Figure 6).

Positivity

The conductivities of neighboring geological features can vary over orders of magnitude, with the relative differences between conductivities being significant. It is therefore natural to invert for the logarithms of the conductivities rather than the conductivities themselves. This ensures that the conductivities in the constructed model are positive. In contrast, the absolute differences between susceptibilities tend to be diagnostic in the exploration context. So we choose to invert for susceptibility rather than the logarithm of susceptibility. Also, the appropriate reference susceptibility model is most often a half-space of zero SI units, which cannot be included properly if the model is the logarithm of susceptibility. However, most materials giving rise to magnetic effects have nonnegative susceptibility, so we impose the constraint that the susceptibilities in the constructed model should be positive.

We follow the practice of Li and Oldenburg (2003) and impose the positivity constraint on the susceptibilities by including a logarithmic barrier term in the objective function. The underlying inverse problem considered here, before including the logarithmic barrier term, is nonlinear, unlike that of Li and Oldenburg. However, we have found that applying their formula for the decrease in the coefficient γ of the barrier term has been a successful part of our iterative procedure. The initial value of the coefficient of the logarithmic barrier term is chosen so this component of the objective function is as significant as the combination of the other two components:

$$\gamma^0 = \frac{\phi_d^0 + \beta^0 \phi_m^0}{-\phi_{LB}^0}. \tag{24}$$

As the iterations in the inversion proceed, the coefficient is decreased:

$$\gamma^n = (1 - \min(\lambda^{n-1}, 0.925))\gamma^{n-1}, \tag{25}$$

where λ^n is the step length at the previous iteration. This form of the decrease is such that if the inversion is progressing well, and thus the step length is close or equal to 1, the coefficient of the logarithmic barrier term is decreased by about an order of magnitude. If, however, the inversion is struggling, and hence the step length is small, the influence of the logarithmic barrier term remains much the same. Its influence is therefore strong at the early iterations, ensuring that the susceptibilities are significantly greater than zero, but decreases as the inversion progresses, allowing the susceptibilities to approach zero if suggested by the observations. The steady decrease of the coefficient γ for the inversion of the synthetic data set shown in Figure 6 can be seen in Figure 7.

Figure 9 shows the conductivity and susceptibility models constructed by repeating the inversion of the synthetic data set shown in Figure 6 without the positivity constraint on the susceptibilities. All other inversion parameters were the same. The fit to the observations was essentially the same: the final value of misfit was equal to 5.5. As Figure 9b shows, the susceptibility model is similar to Figure 6c, except for a region of small negative values close to the surface. Comparison of the conductivity models constructed by the two inversions (see Figures 6b and 9a) reveals no noticeable difference.

EXAMPLES

Example 1

The first example that we present of the performance of our simultaneous inversion program is mentioned in the Introduction and shown in Figures 3 and 4. This line of data was collected somewhere in Australia. The in-phase and quadrature components of the vertical component of the secondary H-field were measured at three frequencies (1325, 4925, and 11 025 Hz) for a vertical magnetic dipole transmitter. The source and receiver were separated by 5.1 m. The height of the source–receiver pair did not vary much along the line: the average height was 33 m, with a gradual variation between 30 and 36 m. The data shown in Figure 10a (and in Figures 3a and 4a) are the values of the secondary H-field normalized by the z-component of the free-space H-field 5.1 m away from and at the same z-coordinate as the vertical magnetic dipole source. The units are in parts per million (ppm). No estimates of the uncertainties were available for this data set, so values equal to 1 ppm, or 1% of the absolute value of each datum, whichever was larger, were assigned to the observations. These estimates of the uncertainties are shown as the error bars in Figure 10a.

The measurements of the in-phase and quadrature components of the secondary H-field at the three frequencies were made at 105 locations along the line. For each of these locations, the six data values were simultaneously inverted for layered models of both conductivity and susceptibility. The constructed models were stitched together to give the 2D images displayed in Figures 10c and 10d. The forward-modelled data for the constructed model at each sounding location are indicated by the lines in Figure 10a.

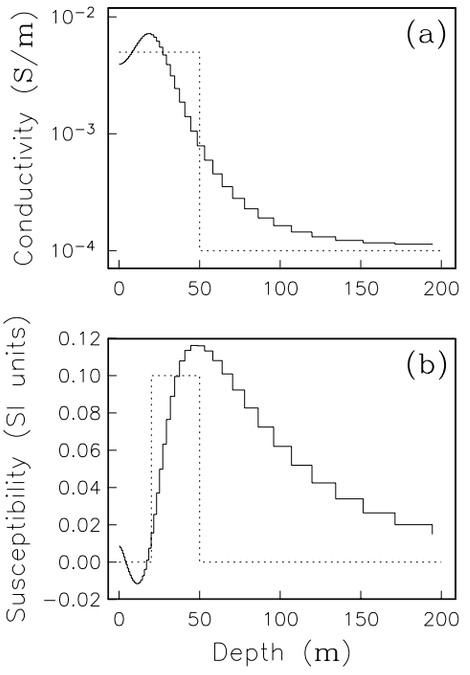

FIG. 9. The constructed models [solid lines; (a) conductivity, (b) susceptibility] for the inversion without the positivity constraint on the susceptibilities of the synthetic data set shown in Figure 6a.

The inversion that produced the results shown in Figure 10 used the GCV-based method for choosing the trade-off parameter at each iteration. The value of the trade-off parameter was not allowed to decrease by more than a factor of two from one iteration to the next to ensure a steady convergence of the iterative procedure. The values of misfit corresponding to the constructed model at each sounding location are plotted in Figure 10b. The ratios of the coefficients for the flattest and smallest components of the model structure term in the objective function were the same: $\alpha_z^\sigma : \alpha_s^\sigma = 1 : 0.01$ and $\alpha_z^\kappa : \alpha_s^\kappa = 1 : 0.01$. The ratio of the coefficients for the conductivity component to those for the susceptibility component was $R^\sigma : R^\kappa = 1 : 100$. The values of the individual coefficients were therefore $\alpha_s^\sigma = 0.01, \alpha_z^\sigma = 1, \alpha_s^\kappa$, and $\alpha_z^\kappa = 100$. Positivity was imposed on the susceptibilities.

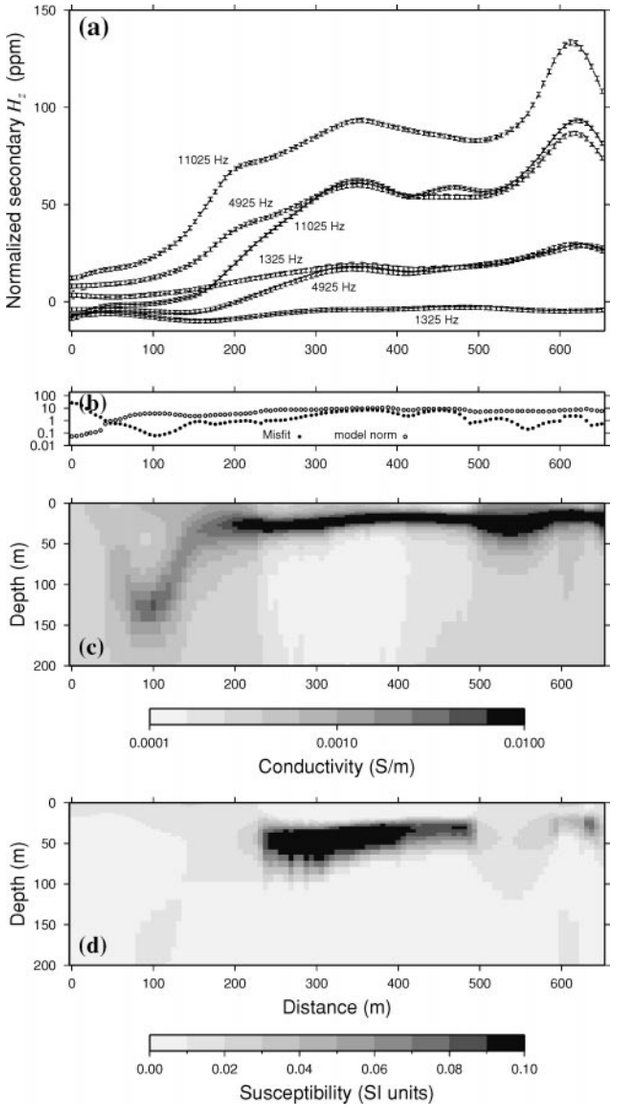

FIG. 10. The result of simultaneously inverting the airborne data in Figure 3 for both conductivity and susceptibility. (a) Observations (error bars) and forward-modelled data (lines) for final model. (b) Misfit (filled circles) and model norm (open circles). (c), (d) Final conductivity and susceptibility models.

The models constructed from the inversion (see Figures 10c and 10d) show a conductive overburden layer along two-thirds of the line over a resistive basement. There is a significant depression and lessening of the conductivity in this layer in the leftmost third of the line (see Figure 10c). The right side of this depression (around 150 m) could be an artifact of the 1D algorithm attempting to fit data from what is actually a termination of the layer at approximately 200 m, although the increase in conductivity at the base of the depression suggests otherwise. The susceptibility model (see Figure 10d) shows a considerable susceptible zone at the base of the overburden in the middle of the line, although the results of the synthetic example (see Figure 6) might suggest that the susceptible zone in Figure 10d extends deeper than the actual susceptible zone. There is small but nonzero susceptibility close to the surface in the left third of the model (similar to the model shown in Figure 8b) that is responsible for reproducing the negative in-phase data at this end of the line. Comparing the conductivity model produced by this inversion with those in Figures 3 and 4 emphasizes how much more information there is in the model constructed by properly inverting the complete data set. In addition, the simultaneous inversion reveals the susceptible region at the base of the surficial layer. As can be seen from the correspondence shown in Figure 10a between the observations and the forward-modelled data for the constructed model, the simultaneous inversion performs very well on this data set which contains significant susceptibility effects. This is emphasized by the small values of misfit along the line (see Figure 10b), which is in marked contrast to the large misfits for the conductivity-only inversion (see Figure 3b). The inversion of the whole line of observations took 20 minutes on a 500-MHz Pentium III computer.

Heath Steele Stratmat

Figure 11a shows airborne data from one of the lines collected at Heath Steele Stratmat near the town of Bathurst, New Brunswick. In this region are several highly conductive and magnetically susceptible massive sulfide deposits and susceptible gabbro dikes. The line of data shown in Figure 11 passes very close to one of the massive sulfide deposits. The data are clearly from a localized 2D or 3D feature. However, we were interested in determining whether the algorithm presented here could produce meaningful results for this data set, which is typical of those in exploration geophysics. Observations were made at three frequencies: 946, 4175, and 4575 Hz. The highest and lowest frequencies were for the coaxial coil configuration, and the middle frequency was for the horizontal coplanar configuration. For both configurations, the transmitter and receiver were separated by 7 m, and their height was approximately 40 m.

The conductivity and susceptibility models obtained from the inversion of the data in Figure 11a are shown in Figures 11c and 11d. The GCV-based method was used to choose the trade-off parameter. Estimates of measurement uncertainties were not available, so uncertainties equal to the greater of 10% of the value of a datum or 1 ppm were assumed. The values of the coefficients in the model structure component of the objective function were $\alpha_s^\sigma = 0.01, \alpha_z^\sigma = 1, \alpha_s^\kappa = 0.1$, and $\alpha_z^\kappa = 1$. The outline of

the mineralized zone at its closest point to the line (50 m to the east) is indicated in Figures 11c and 11d. The highly conductive feature in the constructed model clearly corresponds to the mineralized zone. There is distortion downward and outward from the conductive feature because the inversion is based on a layered representation of the earth. However, considering this, there is good agreement between the constructed image and the location of the mineralized zone: the conductive feature in the constructed model exhibits the southward dip of the mineralized zone and has a comparable thickness. The discrepancy in the depths to the tops of the conductive feature in the model and the mineralized zone is because the mineralized zone is not directly below the observations but is 50 m to the east. Figure 11b shows the values of the misfit and model structure components for the constructed models. At each end of the line, the attained misfits are of the same order as their expected value of 6. Over the mineralized zone, however, the misfits are significantly larger. This is because the GCV criterion has managed to discriminate between the Gaussian noise in the observations and the correlated errors arising from the 1D approximation (Farquharson and Oldenburg, 2003). The result is that the data over the mineralized zone are fit reasonably well and there is meaningful structure in the models, but not fit so closely that the artifacts are extreme.

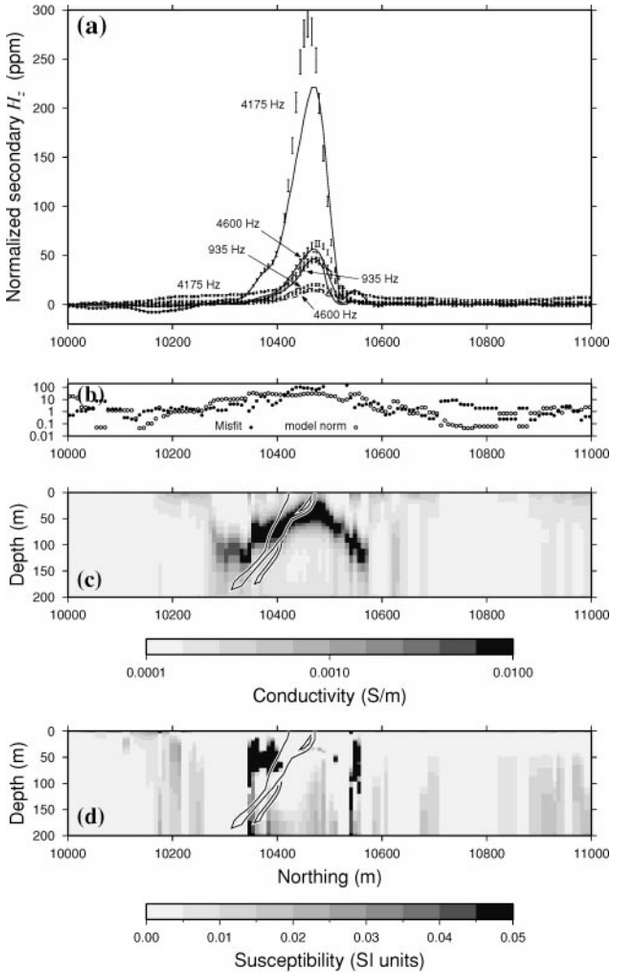

FIG. 11. The results of inverting the line (with easting 12 800 m) of observations from Heath Steele Stratmat closest to the mineralized zone. (a) The error bars indicate the observations, and the lines (solid-in-phase; dashed - quadrature) indicate the forward-modelled data for the models constructed by the inversion. (c) The corresponding conductivity and (d) susceptibility models. (b) The final values of the misfit (solid circles) and model-structure term (open circles). The location of the mineralized zone (50 m to the west of this line) is outlined in (c) and (d).

The data from seven neighboring lines were inverted and the 1D models from all measurement locations were combined to form composite 3D models. The susceptibility model is shown in Figure 12 (upper image) with material of susceptibility less than 0.035 SI units removed. The separation between lines, which was approximately 200 m, is much larger than the spacing of measurements along each line, which was approximately 20 m. The lower image in Figure 12 is of the 3D susceptibility model obtained from the inversion of the ground magnetic data also collected in this area (Li et al., 1996). The cut-off in this image was 0.02 SI units. Comparison of the two images in Figure 12 shows that the values of susceptibility in the model constructed from the EM data are generally larger than those resulting from the inversion of the magnetic data. Nevertheless, there is very good agreement between the features in the two models: the region of susceptibility encompassing the mineralized zone and the east–west-trending susceptible zone in the southern part of the model that is thought to correspond to a gabbro dike.

CONCLUSIONS

When EM induction data are contaminated by the effects of magnetic susceptibility, simultaneous inversion for both

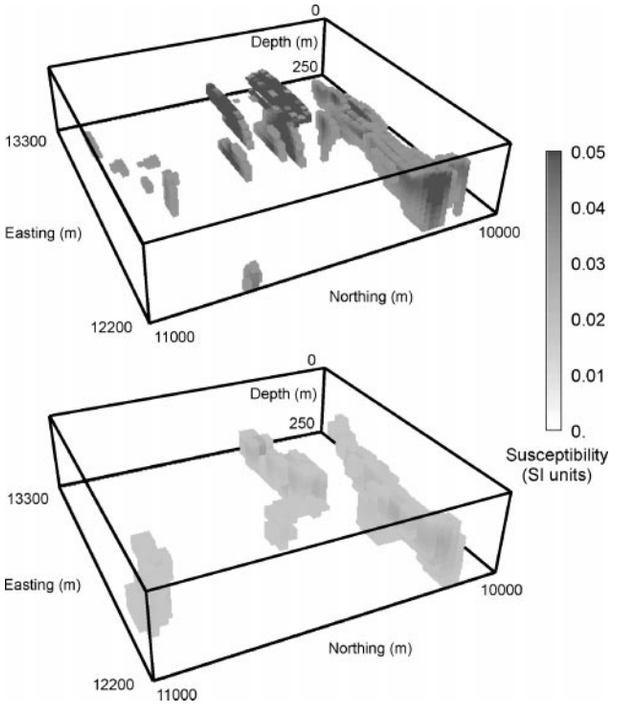

FIG. 12. Volume-rendered views of the susceptibility models constructed from the airborne EM data (upper image) and ground magnetic data (lower image) from Heath Steele Stratmat.

susceptibility and conductivity enables reliable conductivity models to be constructed. If the susceptibility effects are strong enough, information about the variation of susceptibility within the earth can also be obtained. Such information would complement any model obtained from the inversion of static magnetic field measurements because of the insensitivity of EM data to remanent magnetization.

Within a minimum structure inversion such as the one presented here, the relative importance of the conductivity and susceptibility parts of the model must be specified. We have presented a simple means of calculating a reasonable initial value for this balance that will give roughly equal importance to both the conductivity and susceptibility parts of the model norm. What value actually gives the most appropriate conductivity and susceptibility models is problem dependent and for the user to determine. However, even though the susceptibility model might change considerably as the balance of the two parts of the model norm changes, the conductivity model remains virtually the same.

Finally, methods such as the GCV criterion which automatically estimate the trade-off parameter during the course of an inversion enable appropriate fits to be made to data sets even when good estimates of the noise in the observations are lacking.

ACKNOWLEDGMENTS

We thank Robert Smith (formerly of Rio Tinto, now of Greenfields Geophysics) for providing us with the data set from Australia. We also thank Esben Auken, David Fitterman, Hansruedi Maurer, and an anonymous reviewer for their thorough reviews of this manuscript, of which we are most appreciative. The work presented here was funded by NSERC and the IMAGE Consortium, of which the following were members: AGIP, Anglo American, Billiton, Cominco, Falconbridge, INCO, MIM, Muskox Minerals, Newmont, Placer Dome, and Rio Tinto. We are grateful for their participation. Finally, we thank Roman Shekhtman for his assistance with all computer-related matters.

REFERENCES

Anderson, W. L., 1982, Fast Hankel transforms using related and lagged convolutions: ACM Trans. Math. Software, **8**, 344–368.

Beard, L. P., and Nyquist, J. E., 1998, Simultaneous inversion of airborne electromagnetic data for resistivity and magnetic permeability: Geophysics, **63**, 1556–1564.

Farquharson, C. G., and Oldenburg, D. W., 1993, Inversion of time-domain electromagnetic data for a horizontally layered earth: Geophys. J. Internat., **114**, 433–442.

——— 1996, Approximate sensitivities for the electromagnetic inverse problem: Geophys. J. Internat., **126**, 235–252.

——— 2003, A comparison of L-curve and GCV techniques for estimating the regularization parameter in nonlinear inverse problems: Geophys. J. Internat., in press.

Gill, P. E., Murray, W., and Wright, M. H., 1981, Practical optimization: Academic Press Inc.

Haber, E., and Oldenburg, D. W., 2000, A GCV based method for nonlinear ill-posed problems: Computa. Geosci., **4**, 41–63.

Hansen, P. C., 1998, Rank-deficient and discrete ill-posed problems: Numerical aspects of linear inversion: Soc. Ind. Appl. Math.

Huang, H., and Fraser, D. C., 1998, Magnetic permeability and electrical resistivity mapping with a multifrequency airborne EM system: Expl. Geophys., **29**, 249–253.

——— 2000, Airborne resistivity and susceptibility mapping in magnetically polarizable areas: Geophysics, **65**, 502–511.

Li, Y., and Oldenburg, D. W., 1999, 3-D inversion of dc resistivity data using an L-curve criterion: 69th Ann. Internat. Mtg., Soc. Expl. Geophys., Expanded Abstracts, 251–254.

——— 2003, Fast inversion of large-scale magnetic data using wavelet transforms and a logarithmic barrier method: Geophys. J. Internat., **152**, 251–265.

Li, Y., Oldenburg, D. W., Farquharson, C. G., and Shekhtman, R., 1996, Inversion of geophysical data-sets at Heath Steele Stratmat: JACI Consortium Annual Report for 1995, Univ. of British Columbia.

McGillivray, P. R., and Oldenburg, D. W., 1990, Methods for calculating Fréchet derivatives and sensitivities for the non-linear inverse problem: A comparative study: Geophys. Prosp., **38**, 499–524.

Mitsuhata, Y., and Uchida, T., 2000, 2.5-D inversion of frequency-domain CSEM data based on quasi-linearized ABIC: 70th Ann. Internat. Mtg., Soc. Expl. Geophys., Expanded Abstracts, 312–315.

Paige, C. C., and Saunders, M. A., 1982, Algorithm 583, LSQR: Sparse linear equations and least-squares problems: ACM Trans. Math. Software, **8**, 195–209.

Uchida, T., 1993, Smooth 2-D inversion for magnetotelluric data based on statistical criterion ABIC: J. Geomag. Geoelectr., **45**, 841–858.

Wahba, G., 1990, Spline methods for observational data: Soc. Ind. Appl. Math.

Wait, J. R., 1953, A conducting permeable sphere in the presence of a coil carrying an oscillating current: Can. J. Physics, **31**, 670–678.

Ward, S. H., and Hohmann, G. W., 1988, Electromagnetic theory for geophysical applications, *in* Ed., Nabighian, M. N., Electromagnetic methods in applied geophysics: Soc. Expl. Geophys., 131–311.

Zhang, Z., and Oldenburg, D. W., 1999, Simultaneous reconstruction of 1-D susceptibility and conductivity from electromagnetic data: Geophysics, **64**, 33–47.

Zhdanov, M. S., and Pavlov, D. A., 2001, Analysis and interpretation of anomalous conductivity and magnetic permeability effects in time domain electromagnetic data, part II: Sμ-inversion: J. Appl. Geophys., **46**, 235–248.

APPENDIX

SENSITIVITY CALCULATIONS

Our forward-modeling procedure follows the matrix propagation formulation presented in Appendix C of Farquharson and Oldenburg (1996). The procedure uses the z-component of the Schelkunoff **F**-potential discussed byWard and Hohmann (1988). This is the only component of the two Schelkunoff potentials required when calculating, under the quasi-static assumption, the fields for horizontal as well as vertical magnetic dipole sources above a layered model.

As an example of the expressions for the components of the H-fields, consider the z-component at some point (x, y, z) above the surface of the layered-earth model ($z = 0$ on the surface with z positive downward) resulting from a unit vertical magnetic dipole source at $(0, 0, -h)$:

$$H_z(x, y, z) = \frac{1}{4\pi} \int_0^\infty \left(e^{-\lambda|z+h|} + \frac{P_{21}}{P_{11}} e^{\lambda(z-h)} \right) \lambda^2 J_0(\lambda r) d\lambda, \tag{A-1}$$

where J_0 is the zero-order Bessel function and $r^2 = x^2 + y^2$. The terms P_{21} and P_{11} are elements of the propagation matrix

$$\mathbf{P} = \mathbf{M}_1 \prod_{j=2}^{M} \mathbf{M}_j \tag{A-2}$$

(see equation C18 of Farquharson and Oldenburg, 1996), where $\mathbf{M}_j$ is the individual propagation matrix for layer j. We compute the Hankel transforms in equation (A-1) and the expressions for the other components of the H-fields using the digital filtering routine of Anderson (1982).

The procedure we use for computing the elements of the Jacobian matrix of sensitivities arises from directly differentiating the expressions for the components of the H-field. The procedure ultimately involves the derivatives of the individual layer matrices with respect to the model parameters and the propagation of the matrix equation through the stack of layers, as done for the forward modeling. This is a sensitivity-equation approach (see, e.g., McGillivray and Oldenburg, 1990). All individual layer matrices and the matrices for partial propagation down through the layers are saved during the forward modeling and are reused in the sensitivity computations, making this an efficient process. Also, because this process is based entirely on the forward-modeling procedure, which is stable, and does not involve the additional explicit computation of the electric field at depth (as in an adjoint-equation approach), this is an inherently stable procedure for computing the sensitivities. Finally, the procedures for computing the sensitivities with respect to the conductivities and the susceptibilities are directly analogous to each other. Below, we summarize the derivation of relevant expressions required by our procedure for the sensitivity computations.

Consider, for example, the z-component of the H-field for a z-directed magnetic dipole as given by equation (A-1). The only part of this expression that depends on the model parameters is the coefficient P_{21}/P_{11}. The sensitivity of H_z for a vertical dipole source with respect to the model parameter m_j (either the conductivity or the susceptibility of the jth layer) is therefore given by

$$\frac{\partial H_z}{\partial m_j}(x, y, z) = \frac{1}{4\pi}\int_0^\infty \left(e^{-\lambda|z+h|} + \frac{\partial}{\partial m_j}\left[\frac{P_{21}}{P_{11}}\right] e^{\lambda(z-h)} \right) \times \lambda^2 J_0(\lambda r) d\lambda. \tag{A-3}$$

The derivative of the coefficient is simply

$$\frac{\partial}{\partial m_j}\left[\frac{P_{21}}{P_{11}}\right] = \frac{\partial P_{21}}{\partial m_j}\frac{1}{P_{11}} - \frac{P_{21}}{P_{11}^2}\frac{\partial P_{11}}{\partial m_j}. \tag{A-4}$$

The derivative of $\mathbf{P}$ with respect to $m_j (1 \le j \le M-1)$ is

$$\frac{\partial \mathbf{P}}{\partial m_j} = \mathbf{M}_1\mathbf{M}_2, \ldots, \mathbf{M}_{j-1}\left(\frac{\partial \mathbf{M}_j}{\partial m_j}\mathbf{M}_{j+1} + \mathbf{M}_j\frac{\partial \mathbf{M}_{j+1}}{\partial m_j}\right) \times \mathbf{M}_{j+2}, \ldots, \mathbf{M}_M. \tag{A-5}$$

The sensitivities with respect to the conductivity and susceptibility of the basement half-space are given by

$$\frac{\partial \mathbf{P}}{\partial m_M} = \mathbf{M}_1\mathbf{M}_2, \ldots, \mathbf{M}_{M-1}\frac{\partial \mathbf{M}_M}{\partial m_M}. \tag{A-6}$$

The derivatives of the individual layer matrices $\mathbf{M}_j$ with respect to the conductivities and susceptibilities are straightforward to derive and are not given here. The partial propagation matrices

$$\mathbf{P}_k = \mathbf{M}_1\prod_{j=2}^{k}\mathbf{M}_j, \tag{A-7}$$

where $k = 2, \ldots, M$, are computed during forward modeling, and are saved and reused during the sensitivity computations. The Hankel transforms are computed in the same way as for the forward modeling.